Journal Pre-proof

Ratiometric electrochemical immunosensor for the detection of procalcitonin based on the ratios of SiO_2-Fc–COOH–Au and UiO-66-TB complexes

Juncong Miao, Kang Du, Xuan Li, Xiaoting Xu, Xue Dong, Jinglong Fang, Wei Cao, Qin Wei

PII: S0956-5663(20)30701-6

DOI: https://doi.org/10.1016/j.bios.2020.112713

Reference: BIOS 112713

To appear in: *Biosensors and Bioelectronics*

Received Date: 1 June 2020

Revised Date: 22 September 2020

Accepted Date: 7 October 2020

Please cite this article as: Miao, J., Du, K., Li, X., Xu, X., Dong, X., Fang, J., Cao, W., Wei, Q., Ratiometric electrochemical immunosensor for the detection of procalcitonin based on the ratios of SiO_2-Fc–COOH–Au and UiO-66-TB complexes, *Biosensors and Bioelectronics* (2020), doi: https://doi.org/10.1016/j.bios.2020.112713.

Ratiometric electrochemical immunosensor for the detection of procalcitonin based on the ratios of SiO_2-Fc-COOH-Au and UiO-66-TB complexes

Juncong Miao[a], Kang Du[b], Xuan Li[a], Xiaoting Xu[a], Xue Dong[a], Jinglong Fang[a],Wei Cao[a]*, Qin Wei[a]

[a] Collaborative Innovation Center for Green Chemical Manufacturing and Accurate Detection, Key Laboratory of Interfacial Reaction & Sensing Analysis in Universities of Shandong, School of Chemistry and Chemical Engineering, University of Jinan, Jinan 250022, P. R. China

[b] CECEP&CIECC Environmental Investment Management Co.,Ltd., Beijing 100034, China

*Corresponding author.

Dr. Wei Cao

Tel.: +86-53182767890;

fax: +86-53187161600.

E-mail address: jncw88@163.com (W. Cao), jn_chm302@163.com.

Abstract

Procalcitonin (PCT) as a disease marker is of great significance in the early diagnosis of septicemia and pyemia. Biosensor have good prospects for analysis and detection of disease markers, but developing highly sensitive detection methods for detecting PCT remains a daunting task. In this paper, we develop a ratiometric electrochemical immunosensor with Au NPs modified SiO_2-Fc-COOH complex as matrix and UiO-66 loaded with Toluidine blue (TB) as a marker for quantitative detection of procalcitonin (PCT). The SiO_2 modified by APTES not only has a large specific surface area but also contains abundant amino groups, which can be connected to the electrochemical probe of ferrocenecarboxylic acid (Fc-COOH). UiO-66 has the advantages of large specific surface area, high porosity and adjustable structure, which can adsorb toluidine blue electrochemical probe through electrostatic attraction. Measurement and analysis of the prepared immunosensor by Differential Pulse Voltammetry (DPV) show that the oxidation peak currents of Fc-COOH and TB appear at potentials of 0.30 V and -0.30 V respectively. As the PCT concentration increases, the oxidation peak current of TB increases and the oxidation peak current of Fc-COOH decreases. The ratios ($\Delta I=\Delta I_{TB}/\Delta I_{Fc\text{-}COOH}$) between the double signals could show a certain linear relationship with the concentration of the PCT within a certain range. Under optimal conditions, the linear range of detection obtained by the immunosensor was 1 pg/mL-100 ng/mL and the detection limit was 0.3 pg/mL. In this work, the developed ratiometric electrochemical immunosensor not only provides a simple, reliable and sensitive strategy for quantitative detection of PCT but also

provides a useful method for clinical detection of other disease markers.

Keywords: UiO-66-TB, SiO_2-Fc-COOH-Au, PCT, ratiometric electrochemical immunosensor.

1. Introduction

Procalcitonin (PCT) is a polypeptide precursor of calcitonin, consisting of 116 amino acids, which are an effective biomarker for early diagnosis of septicemia and pyemia (Molinero-Fernández et al. 2019; Shen et al. 2015b). The level of PCT in normal human serum is less than 0.1 ng/mL. When the human body is infected with bacteria, it will cause a sharp increase in the level of PCT (Assicot et al. 1993; Karzai et al. 1997; Molinero-Fernández et al. 2019). Therefore, some timely and effective measures can be taken to prevent bacterial infection by monitoring the concentration of the PCT. At present, although some methods for detecting PCT levels have been developed, the analysis of high sensitivity and selectivity for PCT is still a challenge. Therefore, it is of great significance to explore simple, rapid and sensitive PCT detection technology in early disease surveillance.

In recent years, the detection of PCT has made some progress and many methods of detecting PCT have been reported. For instance, electrochemiluminescence (Jia et al. 2019; Xue et al. 2019), fluorescence immunochromatography (Wang et al. 2015a), photoelectrochemical immunosensor (Bao et al. 2019), chemiluminescence (Chen et al. 2018; Yang et al. 2019), electrochemical immunosensor (Fang et al. 2018; Shen et al. 2015a; Yang et al. 2017), surface plasma resonance immunoassay (Vashist et al.

2016). It is worth noting that the electrochemical immunosensor based on the mechanism of specific binding of antigens and antibodies is the product of the development of the interdisciplinary discipline of analytical chemistry and medical biology, which has received close attention from researchers(Li et al. 2015a; Miao et al. 2019; Wang et al. 2015b). It's simple equipment, rapid analysis and high sensitivity detection bring broad prospects for PCT detection.

Electrochemical immunosensors have higher requirements for sensitivity in practical applications, which has prompted researchers to find better electrochemical materials (Chen et al. 2020; Chen et al. 2019a; Chen et al. 2019c). Ferrocene (Fc) and its derivatives are often used as electrochemical signal probes in biosensing devices owing to their good biocompatibility, strong anti-interference ability, and enhanced electronic transmission capability (Chen et al. 2019b; Ma et al. 2016; Sun et al. 2014). Therefore, Fc-COOH with good electrochemical response signal are selected as electrochemical signal probes in immunosensors. A small amount of Fc-COOH is not enough to achieve the desired electrochemical signal strength. Silica nanoparticles (SiO_2) with huge specific surface area can solve this problem (Li et al. 2015b; Xing et al. 2018; Yuan et al. 2010). The SiO_2 surfaces have abundant $–NH_2$ groups modified by (3-aminopropyl) triethoxysilane (APTES) that can provide a universal platform for surface modification via covalent bonds to link the Fc-COOH (SiO_2-Fc-COOH) to further enhance the electrochemical signal (Ning et al. 2019; Trindade et al. 2019). The specific synthesis reaction mechanism is placed in the supporting formation. However, the poor conductivity of SiO_2 will affect the transfer of electrons, resulting

in a decrease in the current signal, which directly affects the sensitivity of the immunosensor. For this reason, the surface of SiO_2 was modified with gold nanoparticles (Au NPs) (SiO_2-Fc-COOH-Au) to increase the overall conductivity of SiO_2 and enhance the electrochemical response signal and improve sensitivity of the immunosensor. The addition of Au NPs not only accelerates electron transfer and improves the conductivity of the material, but also its a large number of active sites can immobilize antibodies and improve electrochemical signals (Ma et al. 2019; Wang et al. 2012). Finally, SiO_2-Fc-COOH-Au is successfully prepared as the matrix of the immunosensor with the electrochemical signal of Fc-COOH and the conductivity of Au NPs.

At the same time, another electrochemical probe, toluidine blue (TB), was successfully loaded into UiO-66 to prepare a biosensor label. Toluidine blue, a member of the water-soluble azine-type redox dye family, has unique chemical and electrochemical properties that lead to their extensive use as electronic mediator in the construction of enzymatic electrodes for biosensing applications (Ribeiro et al. 2018; Wu et al. 2014; Zhang et al. 2018). The following is the mechanism of TB redox reaction (Palakollu and Karpoormath 2018).

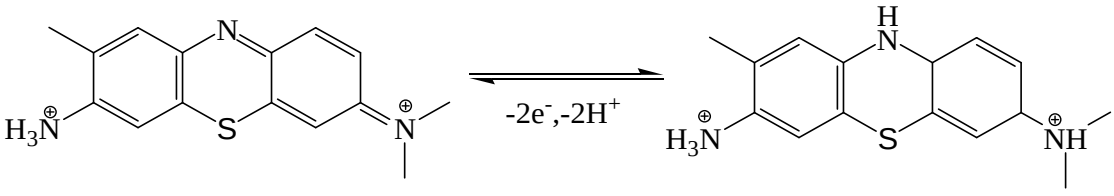

A small amount of toluidine blue is also difficult to achieve the desired intensity of the electrochemical signal. Therefore, the MOF material is selected as the carrier to

carry a large amount of toluidine blue to achieve the purpose of improving the electrochemical response signal. Metal-organic framework materials are crystalline porous materials with periodic network structure formed by self-assembly of metal center and organic ligand (Hu et al. 2015; Zou and Liu 2019). The UiO-66 consists of a cubic framework for cationic $Zr_6O_4(OH)_4$ nodes and 1,4-benzenedicarboxylate (BDC) linkers (Huang et al. 2016; Øien et al. 2014). UiO-66 has the characteristics of large specific surface area, high porosity and easily adjustable structure, which provides a platform for the connection of toluidine blue. TB can be adsorbed on the surface of UiO-66 by electrostatic attraction to solve the problem of weak electrochemical signal of the immunosensor (Wang et al. 2017a).

In this work, we used SiO_2-Fc-COOH-Au as the substrate material and UiO-66-TB as the marker of PCT to construct the ratiometric electrochemical immunosensor. Fc-COOH and TB showed considerable electrochemical signals through Differential Pulse Voltammetry (DPV) detection. Different from classic electrochemical immunosensors which typically adopt the absolute value of the signal as the output, ratiometric electrochemical sensors possess dual electrochemical signals and the quantitative measurement of target was based on the ratio of these two signals. The ratiometric signal readout mode provided a built-in correction factor to eliminate the contribution from non-specific interferences (Yang et al. 2018). The ratiometric electrochemical immunosensor not only had high sensitivity and low detection limit, but also had the characteristics of high accuracy and strong analytical ability. The immunosensor provided a reliable guarantee for the analysis of PCT in this

experiment and provides a new strategy for the analysis of other disease markers.

2. Experimental section

2.1 Materials and reagents

Tetraethoxysilane (TEOS), (3-Aminopropyl) triethoxysilane (APTES) 2-NH_2-terephthalic acid (H2ATA) were obtained from Macklin Biochemical Co., Ltd. (Shanghai, China). Ammonium hydroxide ($NH_3 \cdot H_2O$), $HAuCl_4 \cdot 4H_2O$ (2%), and zircomiun tetrachloride ($ZrCl_4$) were obtained from aladin (Shanghai, China). N, N-Dimethylformamide (DMF), Fc-COOH, HCl (36%-38%) and aceticacid (CH_3COOH) were purchased from the National Medicines Corporation Ltd. of China. PCT and its capture antibody (Ab_1), detection antibody (Ab_2) and bovine serum albumin (BSA, 96-99%) were purchased from Shanghai Linc-Bio Science Co., Ltd. (Shanghai, China). Toluidine blue were purchased from Shanghai Wokai Chemical Reagent Co., Ltd. (Shanghai, China). 1-ethyl-3-(3-dimethylaminopropyl) carbodiimide hydrochloride (EDC) and N-hydroxysuccinimide (NHS) were obtained from Aladdin Reagent Database Inc. (Shanghai, China). Phosphate buffer solution (PBS) was prepared by adjusting the proportion of 1/15 mol/L of Na_2HPO_4 and 1/15 mol/L KH_2PO_4 solution. All other chemicals in the experiment were analytical grade and were used as received without further purification.

The electrochemistry measurements were performed with CHI760D electrochemistry workstation (Chenhua Instrument Shanghai Co., Ltd., China). Fourier Transform Infrared Spectrometer (FT-IR) was recorded by VERTEX70 Spectrometer (Bruker, Germany). X-ray diffraction (XRD) patterns were obtained

using D8 focus diffractometer (Bruker AXS, Germany). Transmission electron microscopic (TEM) image was obtained from a JEOL1400 microscope (Japan). Scanning electron microscope (SEM) images were obtained by a field-emission scanning electron microscope (SEM, Zeiss, Germany). A conventional three-electrode system was employed: the glassy carbon electrode (GCE, 4 mm diameter) as working electrode, the saturated calomel electrode (SCE) as the reference electrode, and the platinum wire electrode as the auxiliary electrode.

2.2 Synthesis of SiO_2-Fc-COOH-Au

The SiO_2 nanosphere were synthesized according to the literature (Zhang et al. 2009). In a beaker, added 9 mL of 28% ammonia water, 16.25 mL of ethanol, and 24.75 mL of ultrapure water. After mixing well, rapidly added 44.5 mL of ethanol containing 4.5 mL of TEOS and reacted at 400 rpm for 2 h at room temperature. Then centrifuged and washed three times with ethanol. Subsequently, the sample was placed in a vacuum oven at 60 °C to dry. Next, we carried out surface amination of silica to prepare SiO_2-NH_2 (Wang et al. 2018). Then, 100 mg of SiO_2 were dispersed in 10 mL ultrapure water. After ultrasonic treatment for 1.5 h, 0.5 mL of APTES was added to the mixture and refluxed at 70 °C for 1.5 h. Then, amino-functionalized silica (NH_2-SiO_2) was obtained and washed several times with ultrapure water and dried under vacuum at 60 °C. Adding Fc-COOH solution (2 mg/mL, 2 mL) to the silica solution (2 mg/mL, 2 mL), then adding EDC (10 mM, 2 mL) and NHS (2 mM, 2 mL) and stirring for 24 h (Feng et al. 2016). The mixture was washed several times with pure water and dried in a vacuum oven at 60 °C. Take a certain amount of

SiO_2-Fc-COOH in a beaker, and 25 mL of Au NPs was added and mixed uniformly. After stirring for 24 hours, centrifuged several times and dried in a vacuum oven at 60 °C. The details of the synthesis of Au NPs were displayed in the supporting formation.

2.3 Synthesis of UiO-66

UiO-66(NH_2) was synthesized by a solvothermal method based on the literature present (Guan et al. 2017). First of place, $ZrCl_4$ (0.056 g), 2-NH_2-benzenedicarboxylate (0.130 g), HCl (0.38 mL) glacial acetic acid (4 mL) and N, N-dimethylformamide (5 mL) are uniformly mixed and transferred to the Teflon-lined autoclave reacting 3 h at 110 ℃. After the reaction, the final sample was cooled to room temperature, separated by centrifugation and washed several times with pure water and ethanol. Finally, the sample is dried in a vacuum oven at 60 ℃.

2.4 Synthesis of UiO-66-TB-Ab_2

After sonicating NH_2-UiO-66 (3.5 mg/mL 1 mL) for 10 min, EDC (10 mmol/L, 1 mL)/NHS (2 mmol/L,1 mL) and Ab_2 of PCT were added to incubate for 12 h at 4 ℃. After centrifugation, the TB (1 mg/mL, 1 mL) solution and EDC (10 mmol/L, 1 mL)/NHS (2 mmol/L,1 mL) were added and incubated again at 4 ℃ for 12 h. After centrifugation, store at 4 ℃.

2.5 Measurement procedure

Prepared electrodes were detected by Different pulse voltammetry (DPV). The DPV scan was performed from -0.6 V to 0.6 V with pulse amplitude of 0.05 V, pulse width of 0.04 s and pulse period of 0.1 s in 10 mL of PBS (0.1 M, pH=7.4).

2.6 Fabrication of the immunosensor

Fig. 1. shows the flow chart of the preparation of the electrochemical immunosensor. First of the place, the surface of GCE was polished by alumina powder and cleaned with ultrapure water. After that the SiO_2-Fc-COOH-Au (6 µL, 2 mg/mL) was modified on the electrode and dried at room temperature. Then, the Ab_1 (6 µL, 1 µg/mL) of the PCT was modified on the electrode. After drying and washing, 3 µL of 1 wt% bovine serum albumin (BSA) was modified on the electrode for eliminating non-specific binding sites. Later washing and drying, PCT (6 µL) was incubated onto the electrode. Afterwards, washing similarly, UiO-66/Ab-TB (6 µL, 3.5 mg/mL) was gradually added to the electrode surface. Finally, the electrode was washed and stored at 4 ℃.

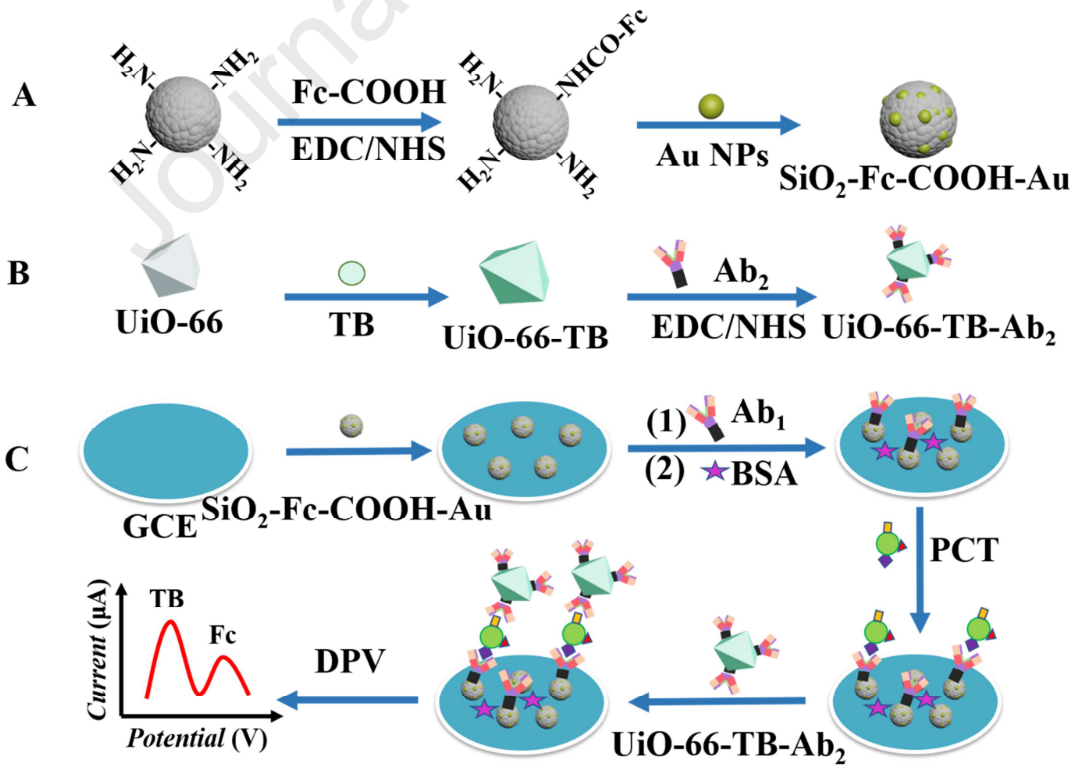

Fig. 1. immunosensor preparation mechanism diagram

3. Results and discussion

3.1 The morphology of materials

As shown in Fig. 2A and Fig. 2B, the morphology of SiO_2 was initially characterized by TEM and SEM. The SiO_2 were uniformly dispersed with a regular spherical shape, which had an average size of about 300 nm. Subsequently, we characterized the morphology of the composite SiO_2-Fc-COOH-Au. As shown in Fig. 2D and Fig. 2E, Au NPs were successfully attached to the surface of silica nanospheres. In addition, the synthesis of SiO_2-Fc-COOH-Au composites was analyzed by infrared spectroscopy. As shown in Fig. 2C, the FTIR spectrum of SiO_2 (a), the adsorption peaks at 3436 cm^{-1} and 1633 cm^{-1} corresponds to the O–H stretching and H–O–H bending vibration of -OH groups and the adsorbed water (Feng et al. 2016). The peak at 2350 cm^{-1} was attributed to the O=C=O asymmetric stretching (Xing et al. 2018). The adsorption peak at 1402 cm^{-1} was caused by C-H bending vibration in the methylene group from APTES (Zou et al. 2014). The strong and wide absorption band at 1101 cm^{-1} was the antisymmetric stretching vibration peak of Si-O-Si (Wang et al. 2015c). The peak at 800 cm^{-1} and 472 cm^{-1} is a Si-O bond symmetric stretching vibration peak (Bodenheimer and Low 1973). The peak at 948 cm^{-1} belonged to the bending vibration absorption peak of Si-OH (Chen et al. 2010). It could be clearly seen from the FTIR of SiO_2-Fc-COOH (b) that the stretching vibration of C=O bond of amide group had a significant absorption peak at 1653 cm^{-1}. The stretching vibration of the C-N bond at 1410 cm^{-1} was also a sign of the amide. The successful combination of SiO_2 and Fc-COOH (SiO_2-Fc-COOH) was

confirmed by FTIR indicating that the materials we needed were successfully prepared.

The morphology of UiO-66 and UiO-66-TB was observed by SEM. As shown in Fig. S1A and Fig. S1B, UiO-66 and UiO-66-TB had a regular octahedral structure. The average size of UiO-66 was 820 m and the size of UiO-66-TB was 800 nm. Compared with UiO-66, the surface of UiO-66-TB becomes rough and easy to adsorb, which confirms that TB was adsorbed on the surface of UiO-66. In addition, UiO-66 was further characterized by XRD. It could be seen from Fig. 2F, curve a was the XRD of the standard UiO-66 obtained from the calculation of the Cambridge crystal database structure diagram (The Cambridge Crystallographic Data Centre, access structures 1405751). All peaks in curve b were highly matched to standard simulated XRD peaks indirectly proved the successful preparation of UiO-66 material (Chakarova et al. 2019; Lemaire et al. 2017; Wang et al. 2017).

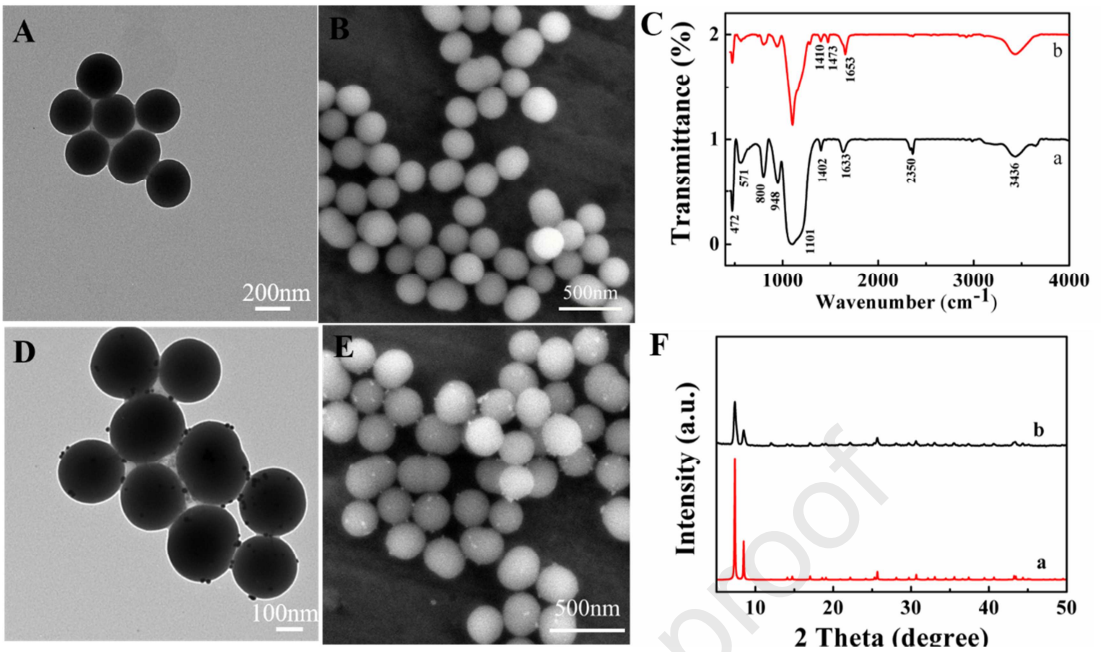

241 **Fig. 2.** TEM image of SiO_2 (A) and SEM image of SiO_2 (B); (C) FTIR spectrum of SiO_2 (a),
242 SiO_2-Fc-COOH (b); TEM image of SiO_2-Fc-COOH-Au (D) and SEM image of
243 SiO_2-Fc-COOH-Au (E); (F) XRD pattern of simulated UiO-66 (a) and UiO-66 (b).

244 **3.2 Performance testing of materials**

245 The properties of the materials played a decisive role in the construction of
246 proportional electrochemical immunosensor. In order to verify that the material had a
247 good electrochemical response signal. The comparative test experiment of different
248 materials (GCE (a), SiO_2-Fc-COOH (b), SiO_2-Fc-COOH-Au (c), UiO-66 (d) and
249 UiO-66-TB (e)) was carried out under the same conditions, and the intensity of
250 current signal was obtained through DPV. As shown in Fig. 3A, the bare electrode had
251 no peak current response signal. When modifying a layer of SiO_2-Fc-COOH (6 μL,
252 2.5 mg/mL) on the electrode, the peak current changed significantly at 0.3 V,
253 revealing that Fc-COOH had good redox properties. When modifying the electrode

with a layer of SiO_2-Fc-COOH-Au (6 μL, 2.5 mg/mL), the peak current value increased further. The reason for the increase of peak current was that the addition of Au NPs made the conductivity of SiO_2-Fc-COOH-Au material better and accelerated the electron transfer efficiency. Then, the electrodes modified with UiO-66 (6 μL, 3.5 mg/mL) were examined, and the electrode had almost no peak current. However, when we measured the electrode modified with UiO-66-TB (6 μL, 3.5 mg/mL), we found that the peak current signal was significantly changed, indicating that TB had good redox properties.

3.3 Characterization of the immunosensor

The impedance changed of electrode surface during layer by layer modification could be observed by electrochemical impedance spectroscopy (EIS) (Li et al. 2017). The Nyquist plots of EIS were recorded from 0.01 to 10^5 Hz at 0.151 V in 0.1 M KCl and 2.5 mM $[Fe(CN)_6]^{4-}$/$[Fe(CN)_6]^{3-}$ (Li et al. 2018). The impedance spectrum consisted of a high frequency semi-circular portion and a low-frequency linear portion, the former being related to electron transfer and the latter being related affected by diffusion. As show in Fig. 3B, the curve (a) was the EIS response of bare GCE, the GCE was almost a straight line. The impedance of GCE modified with SiO_2-Fc-COOH-Au (curve b) was not obvious compared to the GCE due to the good electron transport properties of Au NPs. When the electrode was modified with Ab_1, the impedance was considerably increased, indicating that the protein membrane might hinder the electron transfer between the solution and the electrode surface. With the layer by layer modification of BSA, PCT and Ab_2, the impedance value increased,

276 which proved that each layer of material was successfully modified on the electrode.

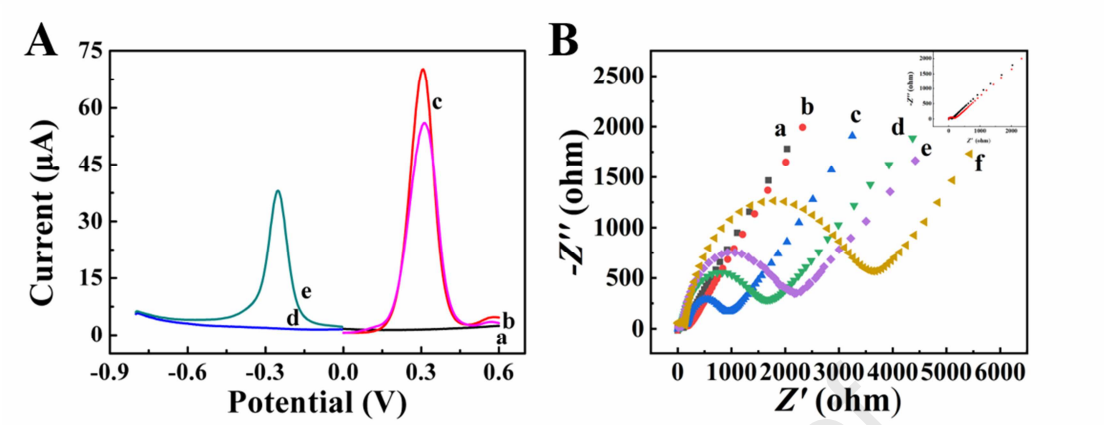

277

278 **Fig. 3.** (A) the peak current response of DPV: GCE (a), SiO_2-Fc-COOH (b) SiO_2-Fc-COOH-Au (c)

279 UiO-66 (d) UiO-66-TB (e); (B) Nyquist plots of the EIS for different modified electrodes (a) GCE,

280 (b) SiO_2-Fc-COOH-Au/GCE, (c) Ab_1/SiO_2-Fc-COOH-Au/GCE, (d)

281 BSA/Ab_1/SiO_2-Fc-COOH-Au/GCE, (e) PCT/BSA/Ab_1/SiO_2-FcCOOH-Au/GCE, (f)

282 UiO-66-TB-Ab_2/PCT/BSA/Ab_1/SiO_2-Fc-COOH-Au/GCE.

283 **3.4 Optimization of experimental conditions**

284 In order to give full play to the analytical performance of the immunosensor, a

285 series of optimizations were carried out for the experimental conditions.

286 The appropriate pH of PBS was related to the survival rate of antigens and

287 antibodies, which had a crucial influence on the sensitive detection of immunosensor.

288 The peak current at different pH was shown in Fig. 4A. From the result, too much

289 acidity or alkalinity would have a certain effect on the electrochemical signal and the

290 optimum pH=7.38 was chosen in the experiment.

291 What's more, the concentration of SiO_2-Fc-COOH-Au played an important role

292 in the experiment. As shown in Fig. 4B, the peak current increased with the
293 concentration of SiO_2-Fc-COOH-Au from 1.0 to 2.5 mg/mL and decreased when the
294 concentration was higher than 2.5 mg/mL. When the concentration of
295 SiO_2-Fc-COOH-Au exceeded the electrode's surface withstand capacity, the electrode
296 surface would gradually become thicker, hindering the transmission of electrons and
297 reducing the electrochemical signal. It demonstrated that the optimal concentration of
298 SiO_2-Fc-COOH-Au was 2.5 mg/mL.

299 In addition, the concentration of UiO-66-TB was of great significance for
300 sensitive detection of immunosensors. As shown in Fig. 5C, the peak current
301 increased with the concentration of UiO-66-TB from 2.0 to 3.5 mg/mL and decreased
302 with the concentration from 3.5 to 4.0 mg/mL. The amount of antigen on the electrode
303 surface was limited. Excessive UiO-66 not only caused waste but also hindered the
304 propagation of electrons and reduced the electrochemical response signal. Therefore,
305 the concentration of UiO-66-TB was 3.5 mg/mL for the best experimental
306 concentration.

307 Besides, the influence of proportion of Au NPs solution on the performance of
308 SiO_2-Fc-COOH-Au was explored. According to the synthesis method of
309 SiO_2-Fc-COOH-Au, a series of SiO_2-Fc-COOH-Au were synthesized by changing the
310 proportion of Au NPs. The synthesized SiO_2-Fc-COOH-Au was detected and studied
311 by cyclic voltammetry. As shown in Fig.S2, with the increase of Au NPs, the
312 conductivity of the material gradually increases, reaching the maximum value at 25
313 mL. The main reason for this phenomenon was that excessive Au NPs was difficult to

effectively load onto the SiO_2-Fc-COOH surface. The corresponding data was placed in the supporting formation.

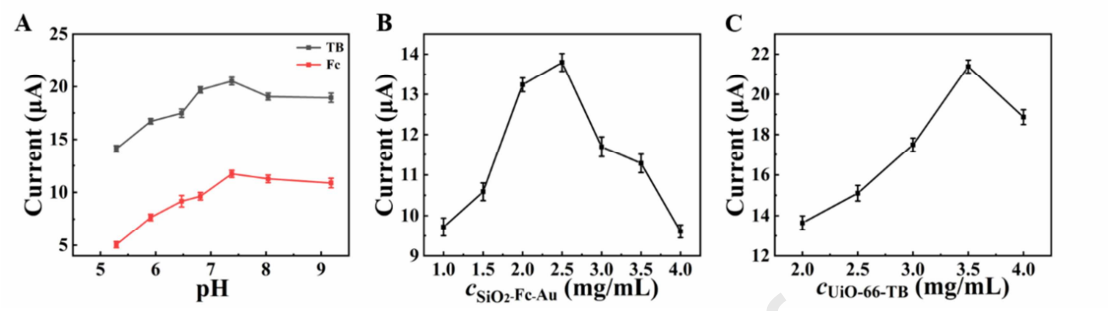

Fig. 4. The optimization of experimental conditions with pH (A) Error bar = SD (n = 5); concentration of SiO_2-Fc-COOH-Au (B) Error bar = SD (n = 3); concentration of UiO-66-TB (C). Error bar = SD (n = 3)

3.5 Analytical performances

Under the optimal experimental conditions, SiO_2-Fc-COOH-Au was used as the substrate, and UiO-66-TB was used as a marker to prepare a ratiometric electrochemical immunosensor for detection PCT concentrations in PBS. The relationship between electrochemical response signals and PCT concentrations was investigated by DPV. As shown in Fig. 5A, with the increase of PCT concentration, the oxidation peak current of TB increased, and the oxidation peak current of Fc-COOH decreased. According to the change of the double signal "$\Delta I=\Delta I_{TB}/\Delta I_{Fc}$" as the response signal for the quantitative determination of PCT concentration. As shown in Fig. 5B, the peak current ratio from 1 pg/mL to 100 ng/mL gradually increased with the increase of PCT concentration. The linear equation between the current ratio and PCT concentration was ΔI =1.85+0.198lg[PCT] (ng/mL) and the correlation coefficient was 0.997 and the limit of detection (LOD) was 0.3 pg/mL (S/N). It was

worth noticing the high sensitivity of the proposed immunosensor after comparison with other previous works, which were listed in Table S1. Favourable sensitivity and accuracy of the prepared ratio-type electrochemical immunosensor benefit from ratiometric strategy. The specific reason was that SiO_2-Fc-COOH-Au and UiO-66-TB underwent redox reactions at different potentials and the generated electrochemical response signals didn't interfere with each other. In addition, SiO_2 and UiO-66 with excellent adsorption properties were used to connect sufficient Fc-COOH and TB signal probes, respectively. At the same time, the introduction of Au NPs not only provides a large number of binding sites for the primary antibody, but also improved the electron transfer rate. Hence, the developed immunosensor could achieve sensitive and stable detection of PCT samples.

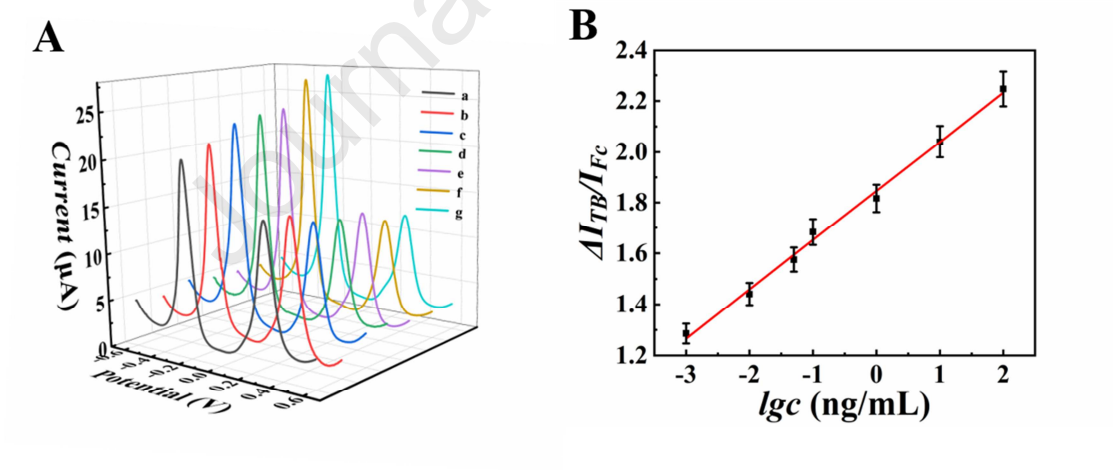

Fig. 5. The immunosensor response to DPV signals for detecting different concentrations of PCT: (a) 1 pg/mL; (b) 10 pg/mL; (c) 50 pg/mL; (d) 100 pg/mL; (e) 1 ng/mL; (f) 10 ng/mL; (g) 100 ng/mL. Error bar = SD (n = 5).

3.6 Selectivity, stability and reproducibility

It was important to study the selectivity, stability and reproducibility of

electrochemical immunosensor for practical application. In this work, uric acid ascorbic acid BSA and PSA were selected as potential interfering substances to study the selectivity of ratiometric immunosensors. As shown in Fig. S3, the presence or absence of the PCT made a significant difference to the electrochemical signal of the immunosensor. Their response of detecting PCT was less than 5% with interfering substances, indicating that the selectivity of the developed immunosensor was acceptable.

To evaluate the reproducibility of the immunosensor, the same five electrodes were prepared for measuring the electrochemical signals generated by 1 ng/mL PCT. As shown in Fig. S4, the standard deviation of the electrochemical signals produced by the electrode was 2.5% and less than 5%, indicating that the sensor had good reproducibility.

To test the stability of the sensor, a series of electrodes were prepared and stored at 4 ℃ when not in use. As shown in Fig. S5, after 15 days, electrochemical signals from SiO_2-Fc-COOH-Au and UiO-66-TB of the immunosensor decreased by 13% and 15%, respectively. The results shown that the stability of the designed immunosensor was acceptable.

3.7 Real sample analyses

To evaluate the accuracy and feasibility of the ratiometric immunosensor in actual sample analysis, different concentrations of PCT were added to human serum samples for analysis in the constructed immunosensors. The results obtained were shown in the Table.1. The concentration of the solution added to the serum was 0.5

ng/mL, 1.0 ng/mL 1.5 ng/mL. The RSD range was 1.93%-3.04% and the recovery ranges from 94.80%-103.20%, showing that the immunosensor had certain potential in the actual detection of PCT. In addition, a comparison experiment with the commercialized available enzyme-linked immunosorbent assay (ELISA) method for the detection of PCT in human serum sample was performed. As Table S7 shown, the relative error between the two methods is in the range from −2.5% to 4.6%, which further demonstrates the ratiometric immunosensor was feasible for analysis in serum samples.

Table. 1 the result of PCT measurement in serum samples

Sample concentration (ng/mL)	Added contents (ng/mL)	Detection content (ng/mL)	RSD (%, n=5)	Recovery (%)
0.5	0.5	0.98, 0.94, 0.97, 0.96, 1.02	3.04	94.80
	1.0	1.47, 1.46, 1.52, 1.44, 1.48,	2.01	97.40
	1.5	2.06, 2.05, 1.98, 2.08, 2.07	1.93	103.20

4 Conclusions

In this work, a ratiometric electrochemical immunosensor was successfully constructed. The electrochemical signals generated by SiO_2-Fc-COOH-Au and UiO-66-TB at different potentials were important for ratiometric immunosensors. In a certain linear range, the ratio immunosensor successfully implements the combination of SiO_2-Fc-COOH-Au and UiO-66-TB electrochemical signal. This immunosensor

not only provided a highly sensitive detection method for PCT, but also provided an effective solution for the analysis of other disease markers.

Acknowledgments

This study was supported by the National Natural Science Foundation of China (No. 21575050), National Key Scientific Instrument and Equipment Development Project of China (No. 21627809), Jinan Scientific Research Leader Workshop Project (2018GXRC024).

References

Assicot, M., Bohuon, C., Gendrel, D., Raymond, J., Carsin, H., Guilbaud, J., 1993. The Lancet 341, 515-518.

Bao, C., Fan, D., Liu, X., Wang, X., Wu, D., Ma, H., Hu, L., Wang, H., Sun, X., Wei, Q., 2019. Biosens. Bioelectron. 142, 111513.

Bodenheimer, J.S., Low, W., 1973. Spectrochim. Acta. A. 29, 1733-1743.

Chakarova, K., Strauss, I., Mihaylov, M., Drenchev, N., Hadjiivanov, K., 2019. Micropor. Mesopor. Mat. 281, 110-122.

Chen, H., Deng, C., Zhang, X., 2010. Angew. Chem. Int. Edit. 49, 607-611.

Chen, P., Qiao, X., Liu, J., Xia, F., Tian, D., Zhou, C., 2018. Sens. Actuators B: Chem. 267, 525-532.

Chen, Y., Ge, X.-Y., Cen, S.-Y., Wang, A.-J., Luo, X., Feng, J.-J., 2020. Sens. Actuators B: Chem. 311,

Chen, Y., Mei, L.P., Feng, J.J., Yuan, P.X., Luo, X., Wang, A.J., 2019a. Biosens. Bioelectron. 145, 111638.

Chen, Y., Wang, A.-J., Yuan, P.-X., Luo, X., Xue, Y., Feng, J.-J., 2019b. Biosens. Bioelectron. 132, 294-301.

Chen, Y., Yuan, P.X., Wang, A.J., Luo, X., Xue, Y., Zhang, L., Feng, J.J., 2019c. Biosens. Bioelectron. 126, 187-192.

Fang, Y., Hu, Q., Yu, X., Wang, L., 2018. Sens. Actuators B: Chem. 258, 238-245.

Feng, T., Qiao, X., Wang, H., Sun, Z., Hong, C., 2016. Biosens. Bioelectron. 79, 48-54.

417 Guan, Q., Wang, B., Chai, X., Liu, J., Gu, J., Ning, P., 2017. Fuel 205, 130-141.

418 Hu, Z., Peng, Y., Kang, Z., Qian, Y., Zhao, D., 2015. Inorganic Chemistry 54,

419 4862-4868.

420 Huang, G., Yang, Q., Xu, Q., Yu, S.-H., Jiang, H.-L., 2016. Angew. Chem. Int. Edit.

421 55, 7379-7383.

422 Jia, Y., Yang, L., Xue, J., Zhang, N., Fan, D., Ma, H., Ren, X., Hu, L., Wei, Q., 2019.

423 ACS Sensors 4, 1909-1916.

424 Karzai, W., Oberhoffer, M., Meier-Hellmann, A., Reinhart, K., 1997. Infection 25,

425 329-334.

426 Lemaire, P.C., Lee, D.T., Zhao, J., Parsons, G.N., 2017. ACS Appl. Mater. Inter. 9,

427 22042-22054.

428 Li, F., Han, J., Jiang, L., Wang, Y., Li, Y., Dong, Y., Wei, Q., 2015a. Biosens.

429 Bioelectron. 68, 626-632.

430 Li, F., Li, Y., Feng, J., Dong, Y., Wang, P., Chen, L., Chen, Z., Liu, H., Wei, Q., 2017.

431 Biosens. Bioelectron. 87, 630-637.

432 Li, F., Li, Y., Feng, J., Gao, Z., Lv, H., Ren, X., Wei, Q., 2018. Biosens. Bioelectron.

433 100, 512-518.

434 Li, Z., Jia, L., Li, Y., He, T., Li, X.-M., 2015b. Applied Surface Science 345, 122-126.

435 Ma, F., Yuan, C.-W., Liu, J.-N., Cao, J.-H., Wu, D.-Y., 2019. ACS Appl. Mater.

436 Inter.11, 19902-19912.

437 Ma, H., Li, Y., Wang, Y., Hu, L., Zhang, Y., Fan, D., Yan, T., Wei, Q., 2016. Biosens.

438 Bioelectron. 78, 167-173.

439 Miao, J., Li, X., Li, Y., Dong, X., Zhao, G., Fang, J., Wei, Q., Cao, W., 2019. Anal.
440 Chim. Acta 1089, 48-55.
441 Molinero-Fernández, Á., Moreno-Guzmán, M., Arruza, L., López, M.Á., Escarpa, A.,
442 2019. ACS Sensors 4, 2117-2123.
443 Ning, S., Zhou, M., Liu, C., Waterhouse, G.I.N., Dong, J., Ai, S., 2019. Anal. Chim.
444 Acta 1062, 87-93.
445 Øien, S., Wragg, D., Reinsch, H., Svelle, S., Bordiga, S., Lamberti, C., Lillerud, K.P.,
446 2014. Cryst. Growth Des. 14, 5370-5372.
447 Palakollu, V.N., Karpoormath, R., 2018. Synthetic Met. 245, 87-95.
448 Ribeiro, J.A., Pereira, C.M., Silva, A.F., Sales, M.G.F., 2018. Biosens. Bioelectron.
449 109, 246-254.
450 Shen, W.-J., Zhuo, Y., Chai, Y.-Q., Yang, Z.-H., Han, J., Yuan, R., 2015a. ACS Appl.
451 Mater. Inter. 7, 4127-4134.
452 Shen, W.J., Zhuo, Y., Chai, Y.Q., Yang, Z.H., Han, J., Yuan, R., 2015b. ACS Appl.
453 Mater. Inter. 7, 4127-4134.
454 Sun, R., Wang, L., Yu, H., Abdin, Z.-u., Chen, Y., Huang, J., Tong, R., 2014.
455 Organometallics 33, 4560-4573.
456 Trindade, E.K.G., Silva, B.V.M., Dutra, R.F., 2019. Biosens. Bioelectron. 138,
457 111311.
458 Vashist, S.K., Schneider, E.M., Barth, E., Luong, J.H., 2016. Anal. Chim. Acta 938,
459 129-136.
460 Wang, H., Wang, H., Chen, S., Dzakah, E.E., Kang, K., Wang, J., Wang, J., 2015a.

Clin. Chim. Acta 444, 37-42.

Wang, H., Zhang, Y., Wang, Y., Ma, H., Du, B., Wei, Q., 2017a. Biosens. Bioelectron. 87, 745-751.

Wang, J., Han, H., Jiang, X., Huang, L., Chen, L., Li, N., 2012. Anal. Chem. 84, 4893-4899.

Wang, Y., Ma, H., Wang, X., Pang, X., Wu, D., Du, B., Wei, Q., 2015b. Biosens. Bioelectron. 74, 59-65.

Wang, Y., Ma, H., Wang, X., Pang, X., Wu, D., Du, B., Wei, Q., 2015c. Biosens. Bioelectron.74, 59-65.

Wang, Y., Wang, L., Huang, W., Zhang, T., Hu, X., Perman, J.A., Ma, S., 2017. J. Mater. Chem. A 5, 8385-8393.

Wang, Y., Zhao, G., Li, X., Liu, L., Cao, W., Wei, Q., 2018. Biosens. Bioelectron. 101, 290-296.

Wu, D., Guo, A., Guo, Z., Xie, L., Wei, Q., Du, B., 2014. Biosens. Bioelectron. 54, 634-639.

Xing, B., Zhu, W., Zheng, X., Zhu, Y., Wei, Q., Wu, D., 2018. Sens. Actuators B: Chem.265, 403-411.

Xue, J., Yang, L., Jia, Y., Wang, H., Zhang, N., Ren, X., Ma, H., Wei, Q., Ju, H., 2019. ACS Sensors 4, 2825-2831.

Yang, L., Fan, D., Zhang, Y., Ding, C., Wu, D., Wei, Q., Ju, H., 2019. Anal. Chem. 91, 7145-7152.

Yang, T., Yu, R.Z., Yan, Y.H., Zeng, H., Luo, S.Z., Liu, N.Z., Morrin, A., Luo, X.L., Li,

W.H., 2018. Sens. Actuators B: Chem.274, 501-516.

Yang, Z.-H., Ren, S., Zhuo, Y., Yuan, R., Chai, Y.-Q., 2017. Anal. Chem. 89, 13349-13356.

Yuan, Y., Yuan, R., Chai, Y., Zhuo, Y., Mao, L., Yuan, S., 2010. J. Electroanal. Chem. 643, 15-19.

Zhang, T., Ma, N., Ali, A., Wei, Q., Wu, D., Ren, X., 2018. Biosens. Bioelectron. 119, 176-181.

Zhang, T., Zhang, Q., Ge, J., Goebl, J., Sun, M., Yan, Y., Liu, Y.-s., Chang, C., Guo, J., Yin, Y., 2009. J. Phys. Chem. C 113, 3168-3175.

Zou, B., Hu, Y., Cui, F., Jiang, L., Yu, D., Huang, H., 2014. J. Colloid Interf. Sci. 417, 210-216.

Zou, D., Liu, D., 2019. Materials Today Chemistry 12, 139-165.

- A ratiometric electrochemical immunosensor was fabricated.
- The electrochemical immunosensor utilized DPV.
- SiO_2-Fc-COOH-Au and UiO-66-TB were used as electrochemical signal probes.
- The designed immunosensor exhibited low detection limit of 0.3 pg mL^{-1} for PCT.

Declaration of interests

☒ The authors declare that they have no known competing financial interests or personal relationships that could have appeared to influence the work reported in this paper.

☐The authors declare the following financial interests/personal relationships which may be considered as potential competing interests: